(Received 29 April 2026, Accepted 3 June 2025, Scheduled 31 August 2026)

Marked Self-Exciting Point Process Modeling of Impulsive Electromagnetic Interference in Power Line Communication Systems

Steven O. Awino* and Bakhe Nleya

Department of Electronic and Computer Engineering, Durban University of Technology, Durban, South Africa

ABSTRACT: Power line communication (PLC) channels are significantly affected by bursty and impulsive electromagnetic interference (EMI), whose temporal clustering and amplitude variability are not adequately captured by conventional statistical models. Existing approaches often treat impulse arrivals and amplitudes independently, limiting their ability to reproduce the coupled dynamics observed in practical transmission line environments. In this study, a marked self-exciting point process model is proposed for PLC noise characterization, where impulse arrival times are governed by a Hawkes-type process, and amplitudes are represented as stochastic marks. The framework incorporates mark-dependent excitation, allowing higher-amplitude impulses to influence subsequent event occurrences and thereby capture the observed bursty structure. A measurement-driven analysis shows that PLC impulsive noise exhibits short-term temporal dependence and deviation from memoryless behavior, as reflected in skewed inter-arrival distributions, nonlinear complementary cumulative distribution function (CCDF) characteristics, and non-zero autocorrelation at small lags. Parameter estimation indicates dominant baseline activity with moderate self-excitation and rapidly decaying temporal influence. Amplitude modeling revealed a skewed distribution with intermittent high-energy events, whereas extreme value analysis using a generalized Pareto distribution suggested a bounded tail behavior for threshold exceedances. A joint likelihood-based estimation framework was developed to enable practical parameter inference. Validation of measured PLC datasets demonstrated that the proposed model consistently captures both temporal and amplitude characteristics without parameter re-estimation. A comparative analysis with a Poisson model showed clear discrepancies, with a quantified CCDF error of 0.15932, highlighting the limitations of memoryless assumptions. Overall, the proposed marked self-exciting framework provides a physically interpretable and statistically consistent representation of impulsive EMI in PLC systems, offering a robust foundation for improved modeling and mitigation strategies.

1. INTRODUCTION

Electromagnetic interference (EMI) in power line communication (PLC) systems, which use existing transmission line infrastructures for data transmission, is predominantly characterized by impulsive disturbances that exhibit irregular, temporal occurrences and significant amplitude variability. These disturbances arise from diverse electromagnetic sources, including switching devices, nonlinear loads, and coupling effects along the transmission medium, resulting in stochastic sequences of impulses with nonuniform spacing and varying intensities [1, 2]. While such interference is often associated with clustering behavior, measurement-driven observations indicate that the dependence between events is primarily short-term rather than persistent. Conventional statistical models for PLC noise, including Middleton Class A formulations and related parametric approaches, typically assume independence between impulse arrival dynamics and amplitude behavior, thereby limiting their ability to represent the coupled nature of the measured EMI processes [3, 4]. This limitation becomes particularly critical in practical PLC systems, where both the timing and magnitude of interference events jointly influence the PLC communication performance and system reliability.

Recent research efforts have explored a range of stochastic and data-driven methodologies to better characterize impulsive EMI in transmission line environments, particularly in the context of emerging smart grid applications. Queueing-theoretic formulations and traffic-based abstractions were proposed to describe burst-like interference arrivals in [5]. However, such approaches often rely on assumptions of stationarity and independence that are not fully consistent with the variability and nonuniform temporal behavior observed in measured PLC noise. Measurement-based studies have demonstrated that PLC interference exhibits significant temporal fluctuations and deviations from idealized statistical assumptions [6], and broader statistical analysis highlights the presence of impulsive characteristics and limitations of conventional modeling approaches in accurately capturing real EMI behavior [7]. Extreme value theory (EVT) has been widely employed to characterize the distribution of high-amplitude disturbances, including PLC impulsive noise, particularly for rare events exceeding a prescribed threshold [8–10]. Although effective in capturing tail behavior, such formulations are inherently static and do not account for the temporal dynamics governing impulse oc-

* Corresponding author: Steven O. Awino (stevena@dut.ac.za).

currence. Bayesian inference frameworks have further enabled improved parameter estimation and uncertainty quantification [11, 12]. However, they typically depend on predefined likelihood structures and do not explicitly incorporate the mechanisms of event interaction or excitation effects. Consequently, existing approaches are limited in their ability to jointly represent temporal and amplitude couplings inherent in impulsive EMI processes.

In addition, nonlinear time-series analysis techniques, including phase space reconstruction [13] and chaos-inspired methods [14], have been applied to EMI signals, revealing structured temporal patterns that deviate from purely random behavior. However, these approaches are primarily diagnostic and do not yield generative stochastic models capable of reproducing both impulse arrival dynamics and amplitude variability. Multifractal and stochastic volatility-based models have also been explored to capture variability and scaling characteristics of PLC noise [1, 3, 4, 15–17], among others. However, such formulations typically focus on continuous-valued processes and do not explicitly represent discrete impulse arrivals or the interaction between event timing and amplitude fluctuations.

Recently, data-driven and hybrid statistical approaches have been proposed for impulsive noise modeling, detection, and mitigation in PLC and related electromagnetic environments, including machine learning-based classification, deep learning architectures, and adaptive filtering frameworks [12, 18–20]. While these methods demonstrate strong performance in detection and suppression tasks, they often operate as black-box models with limited physical interpretability and do not provide explicit probabilistic descriptions of the joint temporal–amplitude dynamics of EMI processes.

Collectively, these limitations reveal a fundamental gap in existing EMI modeling approaches: the absence of a unified, physically interpretable stochastic framework that simultaneously captures temporal dependence, amplitude variability, and extreme event behavior in impulsive noise environments. To address this challenge, this study proposes a marked self-exciting point process model for PLC noise, in which impulse arrivals are governed by a self-exciting mechanism whereas the associated amplitudes are represented as stochastic marks with heavy-tailed characteristics. Unlike Middleton Class A and EVT-based approaches, which primarily model amplitude statistics without explicitly describing temporal dependence, and unlike conventional Hawkes processes, which model event clustering without incorporating amplitude-driven interactions, the proposed framework jointly captures temporal excitation, amplitude variability, and their mutual coupling within a unified probabilistic model. By allowing large-amplitude impulses to influence the likelihood of subsequent events while simultaneously accounting for extreme-value behaviour, the proposed approach provides a physically interpretable representation of bursty impulsive EMI in PLC environments.

The remainder of this paper is organized as follows. Section 2 presents the mathematical formulation of the proposed marked self-exciting point process model for PLC impulsive noise, including the integration of extreme value modeling for high-amplitude events. Section 4 describes the measurement setup, data acquisition procedure, and preprocessing techniques used for impulse detection and event extraction. Section 5 provides the experimental results and discussion, including parameter estimation, temporal and amplitude validation, and a comparative analysis with conventional models. Finally, Section 6 concludes the study.

2. MARKED SELF-EXCITING POINT PROCESS MODEL

2.1. Preliminaries and Notation

EMI in indoor low-voltage PLC systems is modelled as a sequence of discrete disturbance events that occur over a continuous-time observation window $[0, T]$. Therefore, let

$$\mathcal{H}_t = (t_i, m_i) : t_i < t \tag{1}$$

represent the history of the process up to time t, in which $t_i \in \mathbb{R}^+$ denotes the occurrence time of the i-th impulse event, and $m_i \in \mathbb{R}^+$ be its associated mark (which includes amplitude, energy, or envelope magnitude). Therefore, the EMI process can be defined as a marked point process [21–23],

$$(t_i, m_i)_{i=1}^{N(T)}, \tag{2}$$

where $N(T)$ is a counting process that represents the total number of impulses in $[0, T]$. This formulation is physically consistent with PLC noise measurements, where interference exists in discrete impulsive events and has heterogeneous amplitudes and irregular temporal spacing.

The key distinction between the proposed framework and existing impulsive noise models lies in the explicit incorporation of mark-dependent excitation. In conventional Hawkes processes, all events contribute equally to future excitation regardless of their amplitude. In contrast, the proposed model allows high-amplitude impulses to exert greater influence on subsequent arrivals through the term m_i^{β}, thereby establishing a direct coupling between temporal occurrence and impulse severity. This mechanism enables simultaneous characterization of burst formation and amplitude evolution within a single stochastic framework.

2.2. Self-Exciting Structure

To capture the bursty and clustered behaviour of impulsive EMI, a self-exciting (Hawkes-type) conditional intensity function is used to model the arrival process as [21, 22, 24]:

$$\lambda(t \mid \mathcal{H}t) = \mu + \sum t_i < tg(t - t_i, m_i), \tag{3}$$

where $\mu > 0$ defines the baseline (exogenous) intensity, and $g(\cdot)$ denotes the excitation kernel that captures the influence of historical events.

For PLC systems, large-amplitude impulses normally trigger subsequent disturbances (e.g., switching cascades), thus motivating a mark-dependent excitation kernel [23, 24]:

$$g(t - t_i, m_i) = \alpha m_i^{\beta} e^{-\delta(t - t_i)}, \quad t > t_i, \tag{4}$$

where α, β, $\delta > 0$.

As such, the intensity becomes,

$$\lambda(t \mid \mathcal{H}t) = \mu + \sum t_i < t\alpha m_i^\beta e^{-\delta(t-t_i)}. \tag{5}$$

In this formulation in PLC context, μ defines the background EMI resulting from persistent sources; m_i^β denotes the strong impulses inducing higher excitation; $e^{-\delta(t-t_i)}$ is the memory decay that reflects transient coupling effects. This structure allows the modeling of EMI burst generation, which is a well-documented feature of PLC noise.

2.3. Mark (Amplitude) Distribution

The amplitude of impulsive EMI is characterized by heavy-tailed behavior, confirming the existence of rare but extreme disturbances. To capture both moderate and extreme EMI events, a hybrid mark model was adopted [25, 26]:

$$m_i \sim \begin{cases} f_{\text{bulk}}(m;\theta_b), & m \le u, \\ f_{\text{tail}}(m;\theta_t), & m > u, \end{cases} \tag{6}$$

where u is a predefined threshold. For

(a) Bulk component resulting from routine switching noise, a lognormal distribution is employed:

$$f_{\text{bulk}}(m) = \frac{1}{m\sigma\sqrt{2\pi}} \exp\left(-\frac{(\ln m - \mu_b)^2}{2\sigma^2}\right). \tag{7}$$

(b) Tail component (EVT) characterized by rare high-energy transients (e.g., arcing, load switching) for $m > u$, the Generalized Pareto Distribution (GPD) is used:

$$f_{\text{tail}}(m) = \frac{1}{\sigma_t}\left(1 + \xi\frac{m-u}{\sigma_t}\right)^{-\left(1+\frac{1}{\xi}\right)}, \tag{8}$$

where ξ and σ_t define the shape and scale parameters, respectively.

2.4. Joint Likelihood Function

Let $(t_i, m_i)_{i=1}^{N(T)}$ be an observation of a marked point process. Then, the likelihood function is defined as [21, 22, 27],

$$\mathcal{L} = \left[\prod_{i=1}^{N(T)} \lambda(t_i \mid \mathcal{H}t_i) \cdot f(m_i \mid \mathcal{H}t_i)\right] \exp\left(-\int_0^T \lambda(t \mid \mathcal{H}_t), dt\right). \tag{9}$$

The step-by-step decomposition and definition of (9) is as follows:

(a) The arrival contribution is given by,

$$\prod_{i=1}^{N(T)} \lambda(t_i \mid \mathcal{H}_{t_i}) \tag{10}$$

(b) The mark contribution is as,

$$\prod_{i=1}^{N(T)} f(m_i \mid \mathcal{H}_{t_i}) \tag{11}$$

(c) The compensator (normalization term) is defined by,

$$\exp\left(-\int_0^T \lambda(t \mid \mathcal{H}_t), dt\right) \tag{12}$$

2.5. Evaluation of the Compensator

By substituting the conditional intensity function and using the exponential excitation kernel, the compensator term can be expressed as,

$$\int_0^T \lambda(t), dt = \mu T + \sum_{i=1}^{N(T)} \int_{t_i}^T \alpha m_i^\beta e^{-\delta(t-t_i)} dt \tag{13}$$

Let $s = t - t_i$. Then,

$$\int_{t_i}^T e^{-\delta(t-t_i)} dt = \int_0^{T-t_i} e^{-\delta s} ds = \frac{1 - e^{-\delta(T-t_i)}}{\delta} \tag{14}$$

Thus,

$$\int_0^T \lambda(t), dt = \mu T + \sum_{i=1}^{N(T)} \frac{\alpha m_i^\beta}{\delta}\left(1 - e^{-\delta(T-t_i)}\right) \tag{15}$$

2.6. Log-Likelihood Formulation

The log-likelihood of a marked point process can be formulated as [21, 22, 27],

$$\ell = \sum_{i=1}^{N(T)} \log \lambda(t_i \mid \mathcal{H}t_i) + \sum i = 1^{N(T)} \log f(m_i) - \int_0^T \lambda(t), dt. \tag{16}$$

Substituting the exponential kernel-based conditional intensity, the log-likelihood becomes:

$$\begin{aligned} \ell = {} & \sum_{i=1}^{N(T)} \log\left(\mu + \sum_{t_j < t_i} \alpha m_j^\beta e^{-\delta(t_i - t_j)}\right) \\ & + \sum_{i=1}^{N(T)} \log f(m_i) \\ & - \mu T \\ & - \sum_{i=1}^{N(T)} \frac{\alpha m_i^\beta}{\delta}\left(1 - e^{-\delta(T-t_i)}\right). \end{aligned} \tag{17}$$

This objective function enables joint estimation of

$$\Theta = \mu, \alpha, \beta, \delta, \theta_b, \theta_t. \tag{18}$$

2.7. Model Properties and Physical Interpretation

The model captures the clustering behavior of PLC noise through a self-exciting mechanism that reproduces bursty EMI patterns observed in measurements. Furthermore, it incorporates amplitude–arrival coupling, where the term m_i^β ensures that high-energy impulses increase the likelihood of subsequent events, reflecting the physical dependence between impulse magnitude and occurrence. In addition, heavy-tailed amplitude characteristics were modelled using EVT, enabling an accurate representation of rare but significant interference events critical for system reliability. Importantly, unlike phase space reconstruction (PSR) approaches in [13] or other purely descriptive methods, the proposed framework possesses a generative capability, allowing it to simulate realistic EMI sequences consistent with observed statistical behavior.

2.8. Relation to Existing Models

Existing models capture only partial characteristics of PLC noise. The Middleton Class A model effectively represents amplitude statistics but lacks temporal dependence, while EVT models accurately characterize extreme events yet ignore the underlying event dynamics. Multifractal models account for scaling properties but fail to represent discrete event arrivals, and Hawkes processes successfully capture clustering behavior but typically neglect amplitude variability. In contrast, the proposed model provides a unified framework that integrates these complementary aspects, simultaneously accounting for time dynamics, amplitude statistics, extreme events, and physical interpretability.

2.9. Model Assumptions

In this work, the conditional intensity is assumed to depend only on past events (causality), ensuring that future arrivals do not influence the current excitation process. The associated marks are assumed to be conditionally independent given the event history, while the threshold μ is assumed to be sufficiently high for validating the Generalized Pareto Distribution (GPD) approximation. Furthermore, the excitation kernel is assumed to follow an exponentially decaying form, implying finite-memory behaviour. These assumptions are consistent with measured PLC EMI characteristics and enable tractable parameter estimation and inference. The exponential excitation kernel reflects the observation that the influence of an impulsive EMI event is typically the strongest immediately after occurrence and gradually diminishes with time. In practical PLC environments, impulsive disturbances are commonly generated by switching power supplies, inverter-based converters, motor drives, relay operations, and other nonlinear electrical loads. Such sources frequently produce bursts of closely spaced interference events whose effects persist over short time intervals before decaying. Consequently, the exponential kernel provides a physically meaningful representation of short-term temporal clustering while maintaining computational efficiency.

The proposed mark-dependent excitation mechanism further assumes that larger-amplitude impulses exert greater influence on subsequent event generation than weaker disturbances. This assumption is consistent with practical observations in which high-energy switching and transient events are often accompanied by correlated impulsive activity. As such, the framework establishes a direct coupling between impulse severity and temporal clustering. Despite these advantages, several limitations should be acknowledged. First, the EVT component relies on threshold selection for exceedance extraction. Although threshold sensitivity analysis is performed in this work, the estimated tail parameters may vary when very few exceedances are available. Second, the exponential kernel assumes finite-memory behaviour and may not fully capture long-range dependence or persistent correlations that could arise in highly complex electromagnetic environments. Finally, the model assumes approximately stationary statistical characteristics over the observation interval. In practical smart-grid and power-network environments, varying load conditions may introduce non-stationary behaviour that would require time-varying or regime-switching extensions of the proposed framework.

3. PARAMETER ESTIMATION METHODOLOGY

This section presents the estimation framework for the proposed marked self-exciting point process model, which aims to jointly infer temporal dynamics of impulse arrivals and statistical properties of their amplitudes from observed PLC noise data. Given the derived likelihood structure, parameter estimation is formulated within a maximum likelihood framework, enabling consistent and efficient inference of both the self-exciting intensity and mark distribution parameters. The methodology combines analytical derivations with numerical optimization techniques to ensure tractable, reliable estimation of practical PLC EMI datasets.

3.1. Maximum Likelihood Estimation

Let $\Theta = \mu, \alpha, \beta, \delta, \theta_b, \theta_t$ denote the full parameter vector governing the conditional intensity and mark distributions. Parameter estimation is performed via maximum likelihood by maximizing the log-likelihood function derived in Section 2:

$$\begin{aligned}\ell(\Theta) = & \sum_{i=1}^{N(T)} \log\left(\mu + \sum_{t_j<t_i} \alpha m_j^\beta e^{-\delta(t_i-t_j)}\right) \\ & + \sum_{i=1}^{N(T)} \log f(m_i) - \mu T \\ & - \sum_{i=1}^{N(T)} \frac{\alpha m_i^\beta}{\delta}\left(1 - e^{-\delta(T-t_i)}\right)\end{aligned} \tag{19}$$

This formulation jointly captures temporal clustering using conditional intensity and amplitude variability via the mark distribution. This ensures a unified representation of impulsive EMI in PLC systems. Therefore, this estimation problem can be formulated as,

$$\hat{\Theta} = \arg\max_{\Theta}\ \ell(\Theta), \tag{20}$$

which follows the standard maximum likelihood framework for point processes.

3.2. Practical Optimization Strategy

Due to the nonlinear structure of the log-likelihood, closed-form solutions are unavailable. Therefore, numerical optimization was employed. In this study, a quasi-Newton method is adopted due to its efficiency and robustness for moderate-dimensional problems. To improve convergence, the estimation was performed in two stages:

- Initialization stage
  - Estimate mark distribution parameters independently
  - Initialize temporal parameters using empirical statistics
- Joint optimization stage
  - Refine all parameters simultaneously using the full log-likelihood

This strategy reduces sensitivity to poor initial values and improves numerical stability. The log-likelihood can be separated into two components as follows:

$$\ell(\Theta) = \ell_{\text{time}}(\mu, \alpha, \beta, \delta) + \ell_{\text{marks}}(\theta_b, \theta_t), \tag{21}$$

where the temporal component is derived from the self-exciting point process theory, and the mark component follows standard statistical modeling of amplitude distributions.

3.3. Initialization of Parameters

Initial parameter values are selected based on the data's observable characteristics:

- $\mu \approx N(T)/T$: average impulse rate
- δ: inverse of the mean inter-arrival time
- α: small positive value to ensure stability
- $\beta \approx 1$: Linear amplitude influence (initial assumption)

Mark distribution parameters were estimated using standard methods: the bulk component via lognormal fitting and the tail component via GPD estimation. These initializations provide a physically meaningful starting point for optimization.

3.4. EVT Threshold Selection

The threshold u separating moderate and extreme impulses is selected using established extreme value techniques, including mean excess function analysis and stability of GPD parameter estimates. This ensures that the tail model accurately captures high-amplitude EMI events, which are critical for PLC system performance in the field.

3.5. Algorithmic Implementation

The overall estimation procedure is summarized as follows:

i. Extract the impulse sequence (t_i, m_i) from the PLC signal.

ii. Initialize parameters $\Theta^{(0)}$

iii. Evaluate the log-likelihood $\ell(\Theta)$

iv. Update parameters using a quasi-Newton method

v. Repeat until convergence:

$$|\ell^{(k+1)} - \ell^{(k)}| < \epsilon \tag{22}$$

vi. Output estimated parameters $\hat{\Theta}$

3.6. Computational Considerations

The direct evaluation of the conditional intensity involves the summation over all past events, leading to quadratic computational complexity. To address this, an efficient recursive formulation is employed for the exponential kernel as follows:

$$S_i = e^{-\delta(t_i - t_{i-1})}\left(S_{i-1} + m_{i-1}^{\beta}\right), \tag{23}$$

which reduces computational cost and enables scalable analysis of large PLC datasets. The computational complexity of direct likelihood evaluation is $O(N^2)$ due to summation over previous events. However, the exponential excitation kernel permits recursive intensity updates, reducing the complexity to $O(N)$ and making the framework suitable for efficient PLC noise analysis and potential real-time implementation.

4. DATA DESCRIPTION AND PREPROCESSING

4.1. PLC Noise Measurement Setup

The dataset used in this study consisted of measured impulsive EMI signals collected from a low-voltage PLC environment. The measurements were acquired using a high-resolution Rigol DS2202A digital storage oscilloscope (DSO) connected to the power transmission line network via a differential mode PLC coupler based on the ETSI TS 102 578 standard [28] as shown in Fig. 1. The DSO was set to sample at 1 giga-sample per second, resulting in a 0.014 s window length. This sampling rate was selected to adequately capture fast transient disturbances and impulsive noise components commonly observed in PLC channels.

The measurement setup reflects a realistic operating environment in which EMI is generated by various sources, including switching devices, nonlinear electrical loads, and external electromagnetic coupling. These sources have been confirmed in [17, 29–31] among others to produce impulsive disturbances with irregular temporal spacing and highly variable amplitudes, consistent with observations from measurements, as shown in Fig. 2.

A total of 30 measurement windows were analyzed in this study, each representing a segment of the PLC noise environment under similar operating conditions. For parameter estimation, the extracted impulse sequences from all datasets were

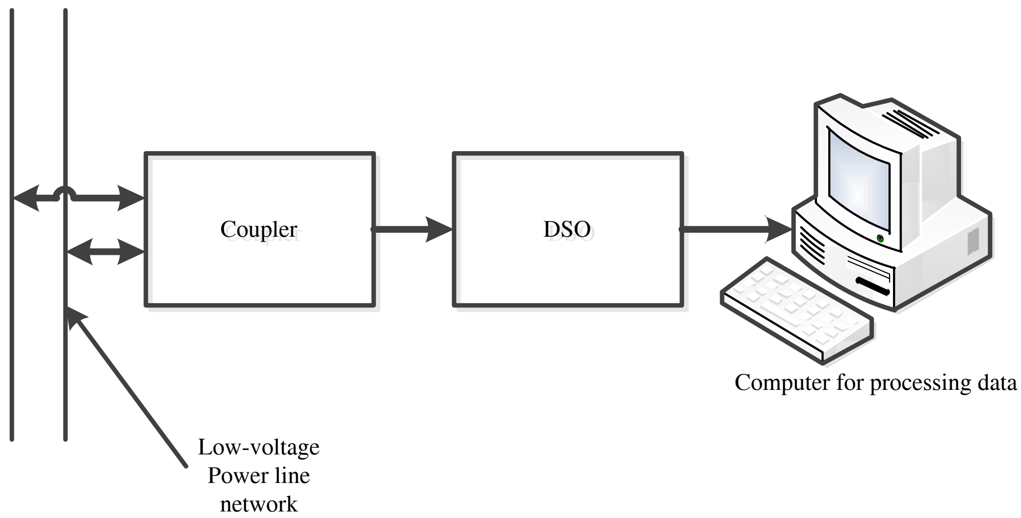

FIGURE 1. Measurement setup [8].

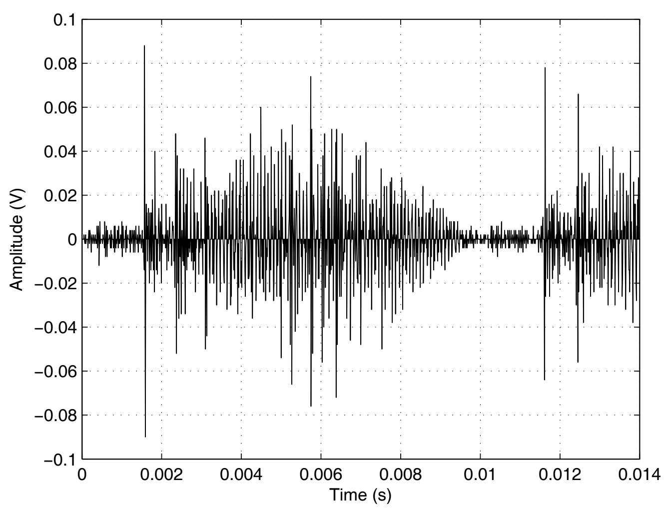

FIGURE 2. Sample impulsive disturbance in PLC network.

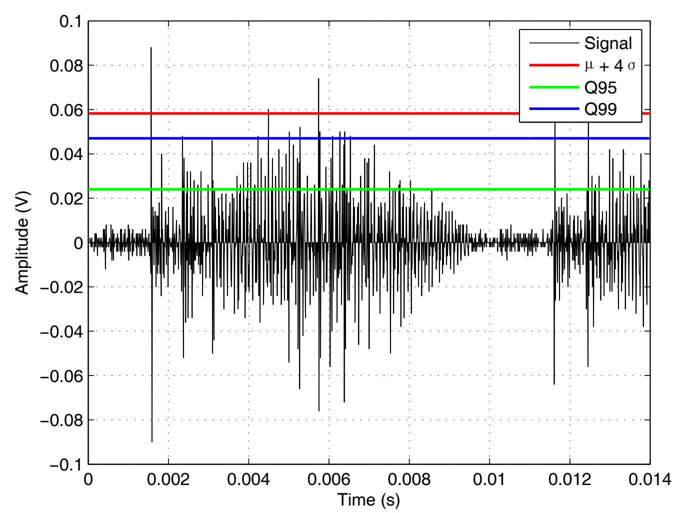

FIGURE 3. PLC noise signal with thresholds (Representative dataset).

aggregated to ensure statistical robustness and sufficient event density for reliable model fitting. Model validation was subsequently performed across individual datasets to assess consistency and generalization of the proposed approach.

4.2. Impulse Detection and Event Extraction

To enable stochastic modeling using the proposed marked self-exciting point process framework, the measured PLC noise waveform was transformed into a sequence of discrete impulsive events. This is achieved through an amplitude-based thresholding procedure, in which significant interference events are identified based on their deviation from the background noise level.

Let $x(t)$ denote the measured EMI signal. An impulse event is detected at time t_i whenever the signal magnitude exceeds a predefined threshold u, that is,

$$|x(t_i)| > u, \tag{24}$$

where t_i corresponds to the local maximum within the exceedance region. The associated mark m_i is defined as the peak amplitude of the detected impulse:

$$m_i = \max_{t \in \mathcal{W}_i} |x(t)|, \tag{25}$$

with $\mathcal{W}_i$ denoting the time window surrounding the i-th exceedance.

The selection of an appropriate threshold is critical because it directly influences the balance between noise suppression and impulse detection. To guide this selection, multiple candidate thresholds were determined based on the statistical characteristics of the measured data, including noise-based threshold $\mu + 4\sigma$ and quantile-based thresholds Q_{95} and Q_{99}. Because 20 datasets were used for training, threshold values were computed individually for each dataset to account for variations in noise characteristics across measurement windows. The results are summarized in Table 1.

In addition, Fig. 3 illustrates the threshold selection on a representative dataset, and Fig. 4 shows the corresponding impulse

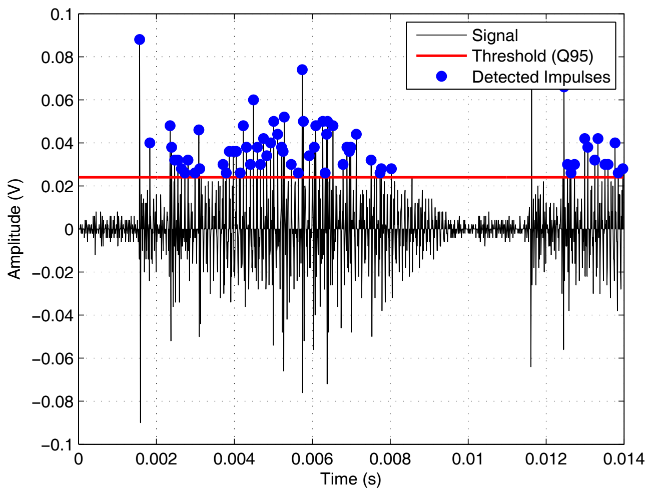

FIGURE 4. Impulse detection in PLC noise signal (Representative dataset).

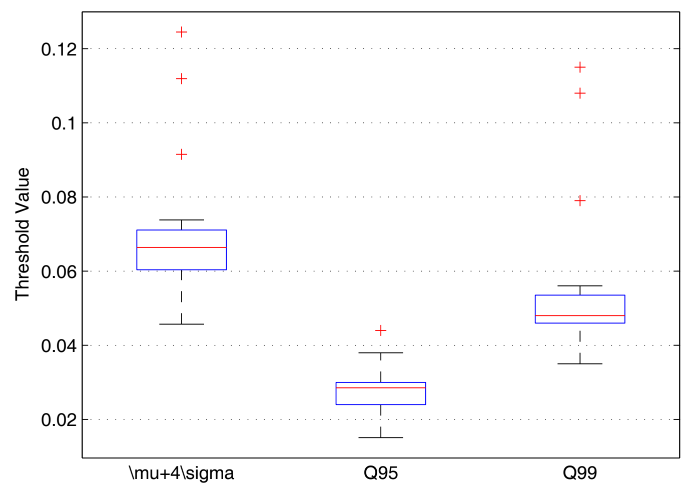

FIGURE 5. Distribution of thresholds across training datasets.

TABLE 1. Threshold analysis results.

Threshold type	Mean	Std Dev	Min	Max
$\mu + 4\sigma$	0.0704	0.0187	0.0457	0.1245
Q_{95}	0.0280	0.0061	0.0151	0.0440
Q_{99}	0.0555	0.0209	0.0350	0.1150

detection results. To assess the consistency across measurement windows, Fig. 5 presents the distribution of thresholds computed over training datasets.

From the analysis, it can be observed that the quantile-based threshold Q_{95} exhibits the lowest variability, with a mean value of 0.0280 and a relatively small standard deviation of 0.0061. This indicates a high degree of consistency across different measurement windows, suggesting that Q_{95} provides a stable and reliable basis for detecting impulses.

In contrast, the noise-based threshold $\mu + 4\sigma$ demonstrated greater variability, with a higher standard deviation (0.0187) and a wider range of values. This increased spread reflects its sensitivity to fluctuations in the underlying noise level, which may lead to inconsistent impulse detections across datasets. Similarly, the Q_{99} threshold, although effective in isolating extreme events, exhibited noticeable variability (standard deviation of 0.0209) and higher threshold values, resulting in sparse event detection. The boxplot further confirms these observations, in which Q_{95} shows a compact interquartile range with minimal dispersion, whereas both $\mu + 4\sigma$ and Q_{99} display broader spreads and outliers. This behavior indicates that the Q_{95} threshold achieves a favorable balance between robustness and sensitivity, enabling consistent detection of impulsive events without being overly influenced by dataset-specific variations.

Based on these results, Q_{95} was selected as the detection threshold for impulse extraction, as it provided sufficient event density for temporal modeling while maintaining stability across measurement conditions. The Q_{99} threshold was retained for extreme value analysis of the amplitude distribution, ensuring accurate characterization of rare, high-energy interference events. The relatively narrow range of Q_{95} values $(0.0151–0.0440)$ further confirms its robustness across varying PLC noise conditions. This approach ensures that the extracted event sequence (t_i, m_i) preserves both the temporal structure and amplitude variability of the measured EMI signal, thereby providing a consistent and physically meaningful input for the marked point process model.

4.3. Statistical Characteristics of PLC Noise

Extracted impulse sequences obtained using the selected detection threshold provide preliminary insight into the statistical structure of PLC electromagnetic interference (EMI), which guides the proposed modeling framework.

As illustrated in Fig. 4, the detected impulses corresponded to distinct high-amplitude excursions superimposed on a lower-level background signal. The use of a moderate quantile-based threshold Q_{95} ensures that both moderate and strong impulsive events are retained, thereby preserving the intrinsic variability of the interference signal and effectively suppressing background noise. This is further supported by the threshold consistency observed across datasets (Fig. 5), which indicates that the adopted detection strategy is stable under varying measurement conditions.

Qualitatively, the detected impulses exhibited intermittent and burst-like behavior, and groups of events appeared within short time intervals separated by relatively quiet periods. This observation suggests the temporal dependence in the EMI process, motivating the use of a self-exciting point process model to capture these clustering effects. In terms of amplitude characteristics, extracted impulse magnitudes span a wide dynamic range, with occasional high-amplitude events that are clearly distinguishable from the bulk of moderate disturbances. This behavior is consistent with heavy-tailed distributions commonly reported in PLC noise and supports to use a higher threshold Q_{99} for extreme value modeling of the amplitude distribution.

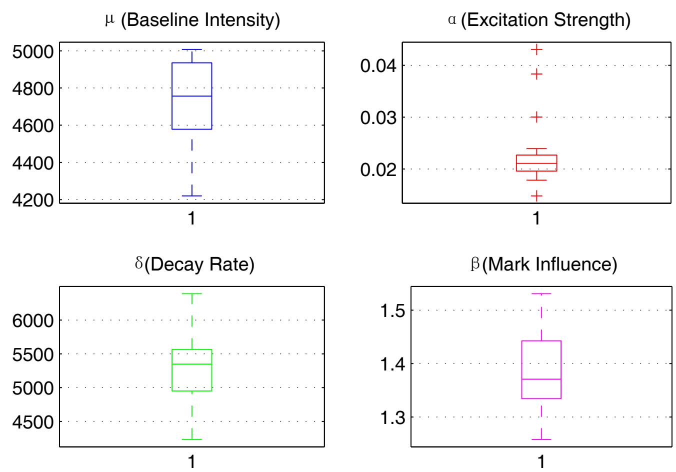

FIGURE 6. Estimated parameters across training datasets.

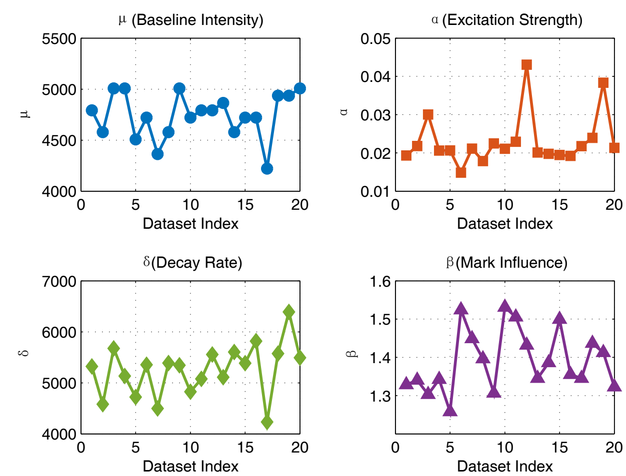

FIGURE 7. Parameter variation across training datasets.

It is important to note that these observations are based on a qualitative inspection of extracted event sequences. A detailed quantitative analysis of inter-arrival times, amplitude distributions, and clustering behavior across both training and validation datasets is presented in Section 5 to rigorously validate these characteristics.

5. RESULTS AND VALIDATION

In this section, the validation of the proposed marked self-exciting point process model using the extracted impulse sequences from the PLC noise datasets is presented. The analysis was conducted using a training–validation approach, in which 20 datasets were used for parameter estimation and the remaining 10 datasets were used for out-of-sample validation.

5.1. Parameter Estimation Results (Training Datasets)

The parameters of the proposed marked self-exciting point process model were estimated using impulse sequences extracted from 20 training datasets. The estimation was performed using maximum likelihood-based formulations with a data-driven initialization to ensure stable convergence across datasets. Fig. 6 presents the distribution of estimated parameters using boxplots, and Fig. 7 illustrates their variation across individual datasets. Table 2 summarizes the corresponding statistical measures, including mean and standard deviation.

TABLE 2. Summary of estimated model parameters (training datasets).

Parameter	Mean	Std Dev
μ (Baseline intensity)	4742.4892	221.5084
α (Excitation strength)	0.0230	0.0068
δ (Decay rate)	5254.5258	503.6194
β (Mark influence)	1.3910	0.0800

The baseline intensity μ exhibited low variability across datasets, with a mean value of 4742.49 and a standard deviation of 221.51. This indicates a consistent background level of impulsive interference in the PLC environment, suggesting that the underlying noise process is largely driven by persistent electromagnetic disturbances. The decay parameter δ had a mean value of 5254.53 with a standard deviation of 503.62, indicating moderate variability across datasets. Notably, δ has a comparable magnitude to μ, implying that excitation effects decay rapidly over time. This behavior is consistent with the short-lived nature of impulsive disturbances in power line communication systems, where interference events typically exhibit limited temporal persistence.

The excitation strength parameter α remained relatively small, with a mean value of 0.0230 and a standard deviation of 0.0068. This suggests that although self-excitation effects are present, they are not dominant, and the overall process is primarily governed by the baseline interference level rather than strong cascade effects. In contrast, the mark influence parameter β demonstrated stable behavior, with a mean value of 1.3910 and a standard deviation of 0.0800. The fact that $\beta > 1$ indicates that higher-amplitude impulses increase the likelihood of subsequent events, confirming amplitude-dependent excitation mechanisms in the PLC noise process.

Overall, the estimated parameters exhibited bounded variability and consistent trends across training datasets, indicating that the proposed model provides a stable and physically interpretable representation of impulsive EMI in PLC systems.

5.1.1. Parameter Uncertainty Analysis

To assess the stability of estimated model parameters, uncertainty analysis was performed across 20 training datasets. Assuming approximate normality of the parameter estimates, 95% confidence intervals were computed according to,

$$CI_{95\%} = \bar{\theta} \pm 1.96 \frac{s_\theta}{\sqrt{N}}, \tag{26}$$

where $\bar{\theta}$ defines the sample mean; s_θ is the sample standard deviation; and $N = 20$ represents the number of training datasets. The resulting confidence intervals are presented in Table 3.

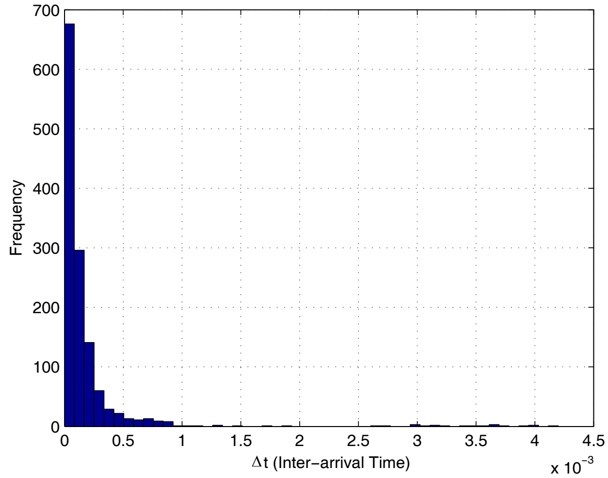

FIGURE 8. Histogram of inter-arrival times in training data.

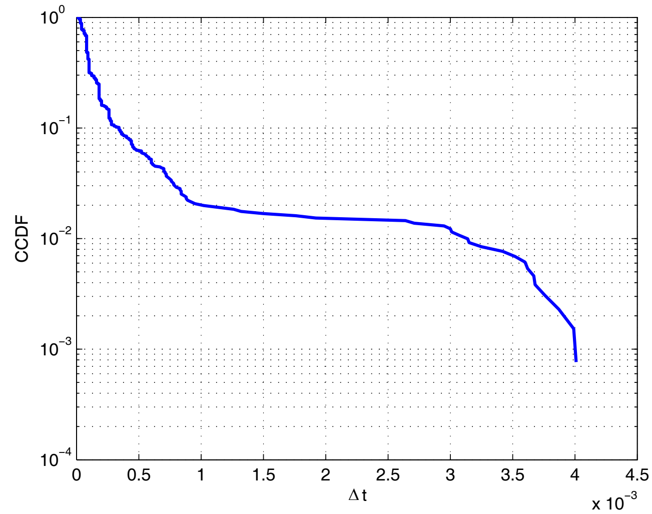

FIGURE 9. CCDF of inter-arrival times.

TABLE 3. Summary statistics and 95% confidence intervals of estimated model parameters.

Parameter	Mean	Std Dev	95% Confidence Interval
μ	4742.4892	221.5084	$[4645.40, 4839.58]$
α	0.0230	0.0068	$[5033.75, 5475.30]$
δ	5254.5258	503.6194	$[0.0200, 0.0260]$
β	1.3910	0.0800	$[1.3560, 1.4260]$

The parameter statistics presented in Table 3 provide information on the stability and robustness of the proposed estimation framework across 20 training datasets. The relatively narrow confidence interval associated with the baseline intensity parameter μ shows a consistent background impulsive activity level across the different PLC noise realizations. Similarly, the excitation decay parameter δ exhibits moderate variability but remains well-constrained, implying that the temporal influence of preceding impulses decays at a relatively consistent rate across datasets. The excitation strength parameter α demonstrates the smallest absolute variation, with a narrow confidence interval indicating stable estimation of the self-excitation effect. In addition, the mark-sensitivity parameter β remains tightly concentrated around its mean value, confirming that impulse amplitudes exert a consistent influence on subsequent event generation. Generally, the relatively narrow confidence intervals observed for all parameters suggest that the proposed marked self-exciting point process yields robust and repeatable parameter estimates, providing confidence in its ability to characterize the temporal and amplitude dynamics of impulsive EMI in PLC environments. The relatively narrow confidence intervals obtained for μ, δ, α, and β indicate that estimated parameters are reasonably stable across training datasets. This suggests that the proposed framework is not highly sensitive to small parameter estimation errors and maintains consistent temporal clustering characteristics.

5.2. Temporal Validation: Inter-Arrival Characteristics

Temporal dynamics of extracted impulse sequences were analyzed to assess the suitability of the proposed self-exciting point process model. Inter-arrival times are computed as $\Delta t_i = t_i - t_{i-1}$ for all detected impulses across training datasets.

Figure 8 presents a histogram of inter-arrival times. The distribution is highly skewed, with a pronounced concentration of short inter-arrival intervals and a gradual decay toward larger values. This indicates that impulsive events frequently occur in rapid succession, whereas longer intervals between events are less common. This suggests that impulse occurrences are not uniformly distributed over time.

The complementary cumulative distribution function (CCDF), shown in Fig. 9, further characterizes this behavior. The empirical CCDF exhibits nonlinear decay, indicating deviation from the exponential behavior, which is typically associated with a memoryless (Poisson) process. The curvature observed in the CCDF suggests that the probability of longer inter-arrival times decreases at a rate inconsistent with independent event arrivals, implying a temporal dependence between impulses.

Figure 10 illustrates the temporal distribution of detected impulses for a representative dataset. The impulse events are not evenly spaced; instead, they appear in dense regions of activity, followed by intervals with reduced event occurrence. Due to the relatively high event density associated with the selected detection threshold, clustering appears as localized concentrations of impulses rather than clearly separated bursts. This reflects the continuous and overlapping nature of impulsive interference in PLC systems.

To complement the visual analysis of the inter-arrival time histogram and CCDF, a Kolmogorov–Smirnov (KS) goodness-of-fit test was performed to evaluate the validity of the memoryless Poisson arrival assumption. Under the null hypothesis, the inter-arrival intervals are assumed to follow an exponential distribution, which is characteristic of a Poisson process. The resulting test statistics are summarized in Table 4.

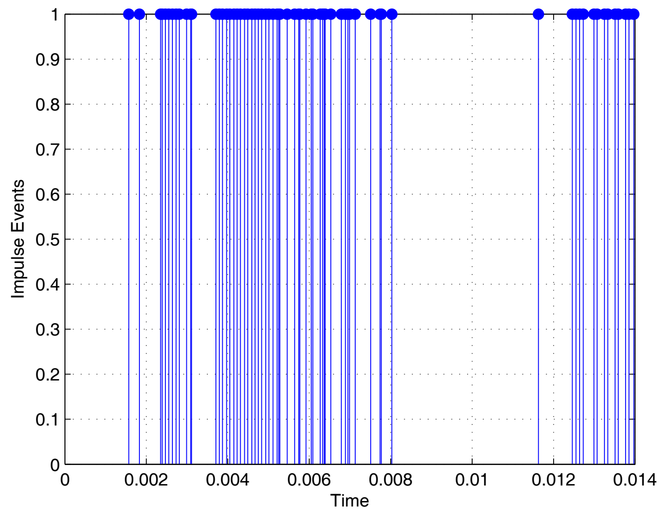

FIGURE 10. Temporal distribution of detected impulses.

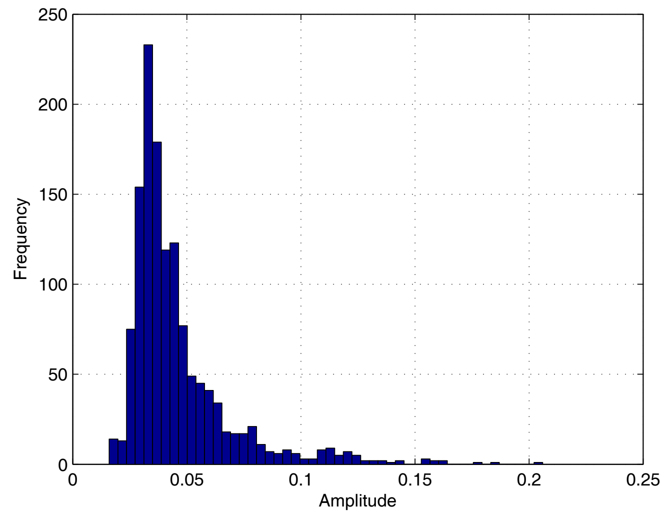

FIGURE 11. Histogram of impulse amplitudes.

TABLE 4. Kolmogorov–Smirnov goodness-of-fit test for the poisson arrival assumption.

Statistic	Value
KS Statistic	0.2768
p-value	< 0.001
Decision	Reject (H_0)
β	1.3910

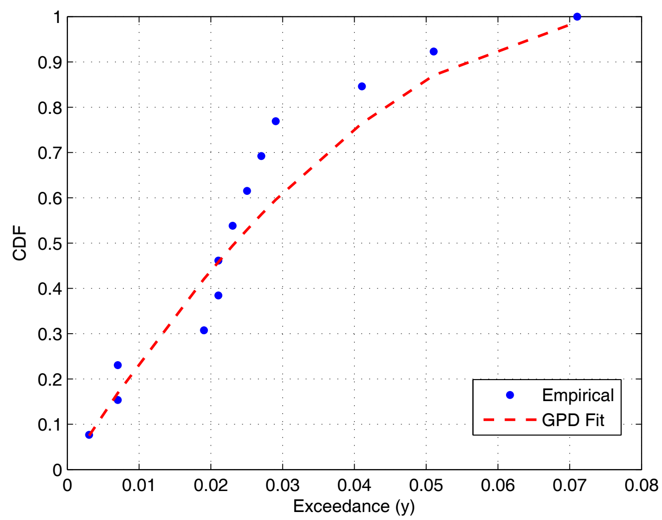

FIGURE 12. GPD fit to amplitude exceedances.

As observed in Table 4, the KS statistic was found to be 0.2768 with a corresponding p-value below 0.001. The relatively large KS statistic indicates a substantial deviation between the empirical inter-arrival distribution and the theoretical exponential distribution. Furthermore, the extremely small p-value leads to rejection of the null hypothesis at conventional significance levels, confirming that the observed impulsive EMI arrivals do not follow a memoryless Poisson process. These results provide quantitative statistical evidence supporting observations from histogram and CCDF analyses, which revealed significant departures from exponential behaviour. The rejection of the Poisson assumption indicates the temporal dependence and clustering effects within the measured PLC noise. From an engineering perspective, this behaviour is consistent with interference generated by switching devices, power electronic converters, inverter-driven loads, and other impulsive electromagnetic sources that tend to produce bursts of closely spaced events rather than independent arrivals. Consequently, the observed arrival dynamics cannot be adequately represented by conventional memoryless models and motivate the adoption of self-exciting point process formulations capable of capturing temporal clustering and event interaction effects.

Collectively, these observations confirm that the impulse arrival process exhibits significant temporal irregularities and clustering behavior. The deviation from exponential inter-arrival characteristics, together with the observed concentration of events over time, provides strong evidence against the assumption of independent arrivals, which captures the dependence of future events on past impulse occurrences.

5.3. Amplitude Validation and Extreme Value Modeling

Amplitude characteristics of detected impulses were analyzed to complement the temporal modeling of PLC noise. The amplitudes m_i, extracted using the detection threshold Q_{95}, were aggregated across the training datasets to examine their statistical behavior. Fig. 11 presents a histogram of impulse amplitudes. The distribution was highly skewed, with a significant concentration of moderate-amplitude events and a gradual decay toward higher values. While most impulses fall within a relatively narrow amplitude range, a small number of larger events extend beyond the bulk of the distribution, indicating intermittent high-energy disturbances.

To further characterize the tail behavior, a higher threshold $u = Q_{99}$ is applied, and exceedances are defined as $y_i = m_i - u$ for $m_i > u$. A total of 13 exceedances were obtained, which were modelled using GPD.

Figure 12 shows the empirical exceedance distribution along with the fitted GPD model. The fitted parameters were $\xi = -0.48007$ and $\sigma = 0.03951$. The negative value of the shape

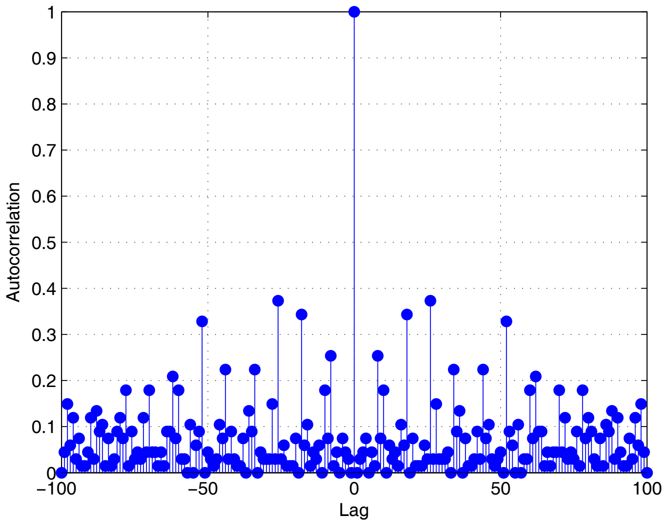

FIGURE 13. Autocorrelation of impulse sequence.

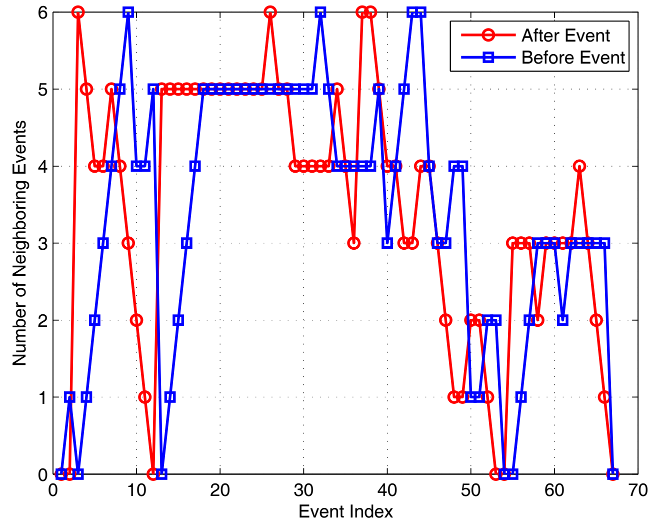

FIGURE 14. Event clustering before Vs after impulse.

parameter ξ indicates that the tail of the amplitude distribution is bounded, implying that while high-amplitude impulses occur, their magnitudes do not grow without bound. Despite the limited number of exceedances, the GPD model provides a reasonable approximation of the empirical distribution, capturing the overall trend of tail behavior. This suggests that extreme amplitude events, although relatively infrequent, can be effectively characterized within a bounded range.

The results demonstrate that PLC impulsive noise exhibits a skewed amplitude distribution with intermittent high-energy events but weak evidence of heavy-tailed unbounded extreme behavior. Therefore, the dual-threshold approach enables the separation of moderate impulses for temporal modeling and higher-amplitude events for tail characterization, providing a comprehensive representation of amplitude dynamics.

5.3.1. Threshold Sensitivity Analysis

To assess the robustness of the EVT-based tail characterization, a threshold sensitivity analysis was performed using the 95th, 97.5th, and 99th percentile thresholds. The resulting GPD parameter estimates are summarized in Table 5.

TABLE 5. Sensitivity of GPD parameters to threshold selection.

Threshold	Exceedances	Shape (ξ)	Scale (σ)
Q_{95}	65	-0.25137	0.03684
$Q_{97.5}$	31	-0.07855	0.02438
Q_{99}	13	-0.49935	0.03985

The number of exceedances decreases from 65 at Q_{95} to 13 at Q_{99}, as expected for increasingly stringent thresholds. Despite this reduction, the estimated shape parameter remains negative across all investigated thresholds, with values ranging from -0.07855 to -0.48007. This consistency indicates that the inferred bounded-tail behaviour is not solely an artifact of the selected threshold but remains stable under reasonable variations in threshold selection. Even though higher thresholds result in fewer exceedances and consequently greater estimation uncertainty, the persistence of a negative shape parameter across all cases provides additional confidence in the EVT-based characterization. The sensitivity analysis therefore supports the conclusion that impulsive EMI amplitudes exhibit a finite upper-tail behaviour within the observed measurement environment.

5.4. Clustering Behavior and Self-Excitation Effects

To further investigate the temporal dependence of impulsive interference, an additional analysis was performed to assess clustering behavior and the presence of self-excitation effects in the extracted impulse sequences.

Figure 13 shows the autocorrelation function of the impulse sequence. A prominent peak is observed at zero lag, as expected, along with noticeable positive correlations at small lags of the two variables. The autocorrelation values decay rapidly as the lag increases, indicating that the dependence between events is primarily short-range. This behavior suggests that impulsive events are temporally correlated within short time intervals but do not exhibit a long-range memory.

Event clustering characteristics were further examined using the number of neighboring events occurring before and after each detected impulse, as shown in Fig. 14. The results indicate comparable levels of activity before and after individual events, with no consistent dominance of post-event activity. This suggests that while some degree of excitation exists, the triggering effect of individual impulses on subsequent events is moderate rather than strong.

Figure 15 shows the distribution of inter-event times for a representative dataset. The distribution is highly skewed, with a large concentration of short intervals and a small number of long gaps. This pattern confirms the burst-like behavior, where impulses tend to occur in clusters separated by relatively quiet periods.

Overall, the results indicate that PLC impulsive noise exhibits short-term clustering with moderate self-excitation. The

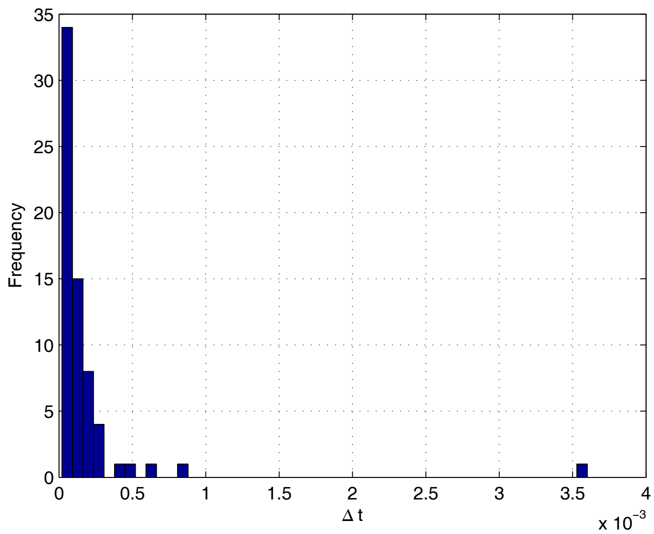

FIGURE 15. Inter-event time distribution.

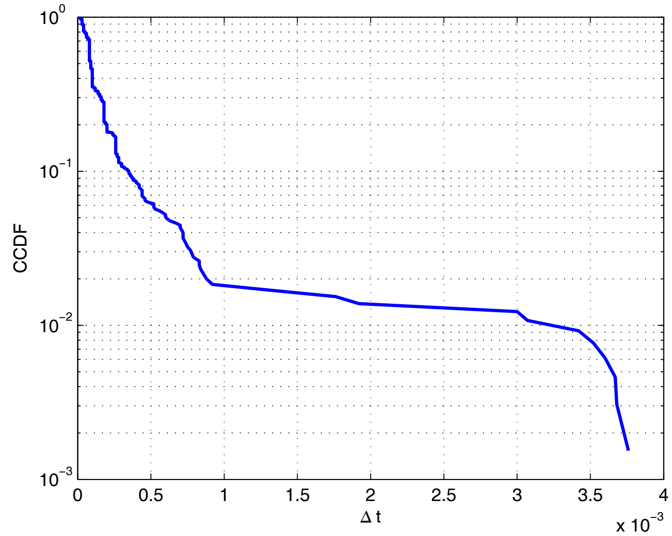

FIGURE 16. Validation data CCDF of Inter-Arrival times.

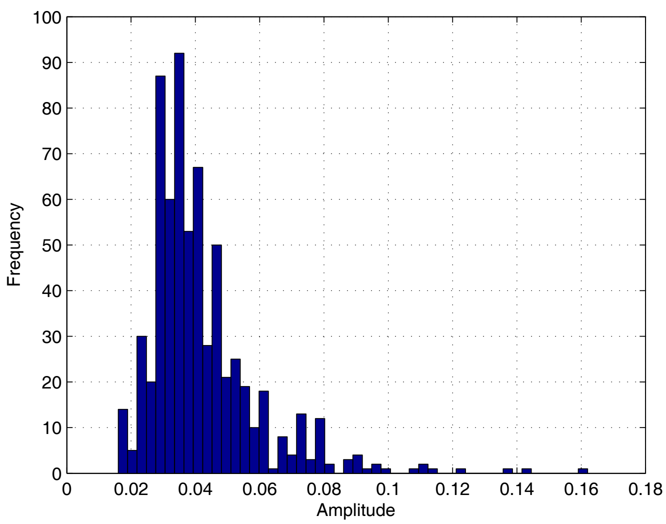

FIGURE 17. Validation data amplitude distribution.

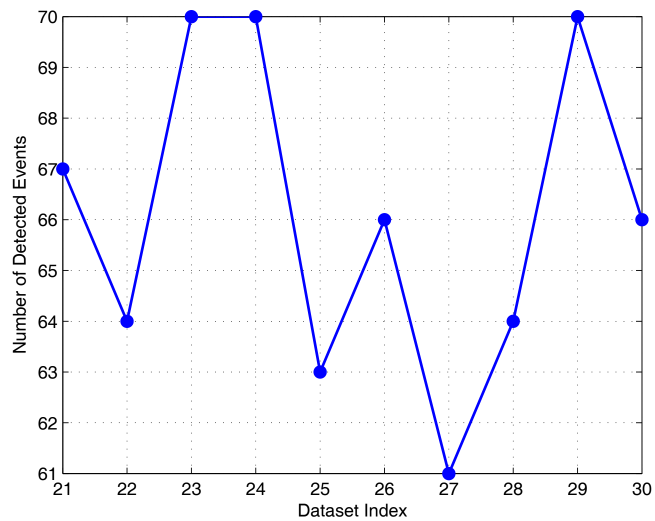

FIGURE 18. Event count across validation datasets.

observed temporal dependence is sufficient to justify using a self-exciting point process model; however, the relatively balanced pre- and post-event activities suggest that the process is not dominated by strong cascade mechanisms. Instead, the impulse arrival process is primarily governed by a combination of background activity and localized temporal interactions.

5.5. Validation on Unseen Datasets

To evaluate the generalization capability of the proposed modeling framework, the analysis was extended to 10 validation datasets that were not used during parameter estimation. The same impulse detection and thresholding procedures were applied without any modification, ensuring a consistent evaluation framework.

Figure 16 presents the CCDF of inter-arrival times for validation datasets. The observed distribution exhibited a similar nonlinear decay pattern to that obtained from the training data, indicating that the temporal characteristics of impulse arrivals remained consistent across datasets. In particular, the concentration of short inter-arrival intervals and the presence of a tail region confirm the persistence of burst-like behavior in the validation dataset.

Figure 17 shows the amplitude distributions of detected impulses. The histogram retained a highly skewed structure, with a dominant concentration of moderate-amplitude events and a gradually decaying tail toward higher amplitudes. This behavior closely matches amplitude characteristics observed in training datasets, indicating that statistical properties of impulse magnitudes are stable under varying measurement conditions.

The consistency of the detection process is further demonstrated in Fig. 18, which presents the number of detected events in validation datasets. The event counts remained within a relatively narrow range, indicating that the threshold-based impulse extraction method was robust and did not introduce significant variability across different measurement windows.

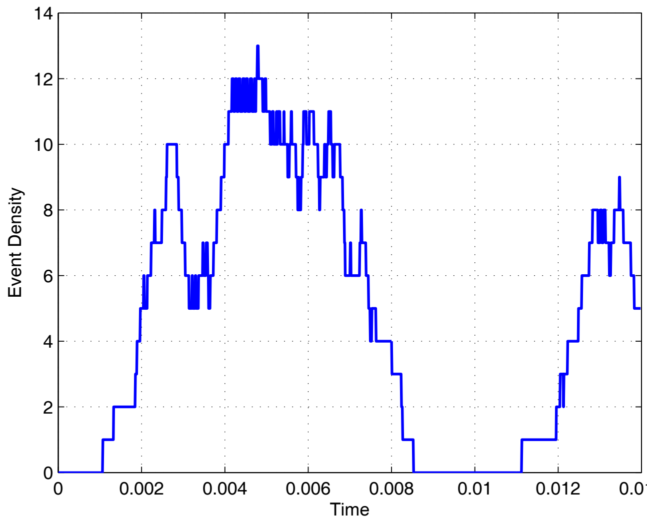

FIGURE 19. Temporal density of impulses.

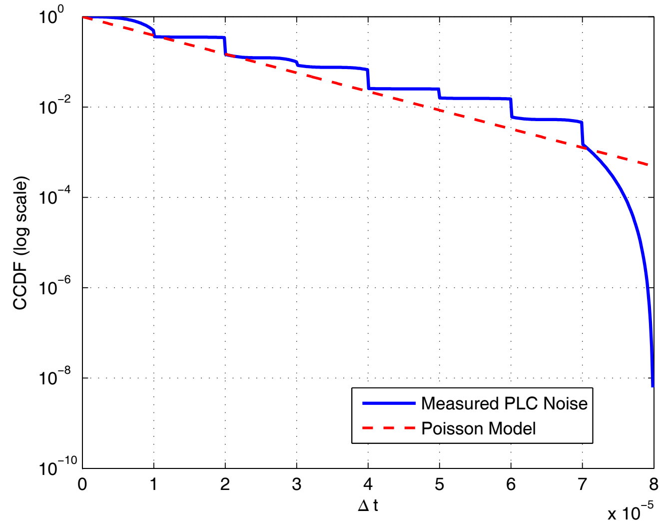

FIGURE 20. Comparison of empirical vs Poisson model.

In addition, the temporal evolution of the impulse activity is illustrated in Fig. 19 using a sliding-window estimate of event density. The plot reveals distinct regions of high and low activity, corresponding to bursts of impulsive interference followed by relatively quiet intervals. This behavior further confirms the temporal clustering and nonuniform event occurrence, which cannot be captured by memoryless models. The observed variation in event density over time supports the need for a modeling framework that accounts for localized temporal interactions between impulses.

Overall, the validation results confirm that both temporal and amplitude characteristics of PLC impulsive noise were consistently captured across unseen datasets. Therefore, the proposed modeling framework demonstrates strong generalization capability, with stable behavior observed in both event dynamics and amplitude distributions without the need for parameter re-estimation.

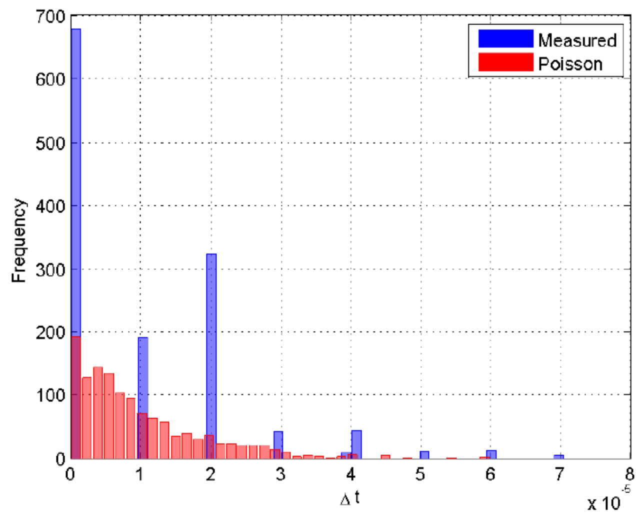

FIGURE 21. Inter-arrival distribution: Real vs Poisson.

5.6. Comparative Analysis with Existing Models

To assess the effectiveness of the proposed marked self-exciting point process model, a comparative analysis was performed against a conventional Poisson process model, which assumes independent and memoryless event arrivals. The comparison focused on temporal characteristics, including inter-arrival distributions, CCDF, and autocorrelation behavior. Fig. 20 presents the CCDF of inter-arrival times for both the measured PLC noise and the corresponding Poisson model. For visualization clarity, the empirical CCDF of the measured data was interpolated using a shape-preserving (pchip) method, which ensured a smooth representation without altering the underlying distribution. The results show a clear deviation between these two models. While the Poisson model exhibits a near-linear decay on the semi-logarithmic scale, consistent with exponential behavior, the measured PLC noise displays a distinct nonlinear profile with slower decay in certain regions and sharper drop-offs at larger inter-arrival times. This indicates that the Poisson assumption fails to capture the temporal dependence of measured data.

To quantify this deviation, the mean absolute error between empirical and Poisson CCDFs was computed, yielding a value of 0.15932. This non-negligible error confirms that the Poisson model provides a poor approximation of the observed inter-arrival behavior.

Fig. 21 shows inter-arrival time distributions for both models. The measured PLC noise exhibited a highly skewed distribution with a strong concentration of short inter-arrival intervals and a heavier tail than the Poisson model. In contrast, the Poisson distribution follows the expected exponential form and lacks the pronounced clustering observed in measured data. This further highlights the inability of the Poisson model to represent bursty interference patterns.

The differences are further emphasized in Fig. 22, which presents the autocorrelation functions of inter-arrival sequences for the two cases. The Poisson model exhibits near-zero autocorrelation across all non-zero lags, confirming its memoryless

TABLE 6. Model comparison using likelihood-based criteria.

Model	Log-Likelihood	AIC	BIC
Poisson	9897.5901	−19793.1802	−19787.9902
Classical Hawkes	10253.5231	−20501.0463	−20485.4765
Marked Hawkes	10222.1670	−20436.3341	−20415.5744

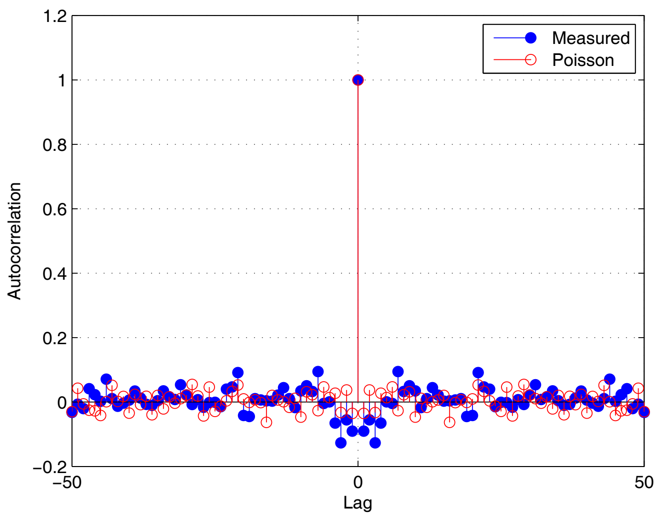

FIGURE 22. Autocorrelation: Real vs Poisson.

nature. In contrast, the measured PLC noise showed small but noticeable positive correlations at short lags, indicating the temporal dependence and short-term clustering effects.

Overall, the comparative analysis demonstrates that the Poisson model is insufficient for accurately characterizing PLC impulsive noise, as it fails to capture the clustering behavior and temporal dependence observed in the data. In contrast, the proposed marked self-exciting point process model provides a more realistic representation by incorporating both event interactions and amplitude effects, thereby enabling improved modeling of bursty EMI in power line communication systems. To further quantify model adequacy, likelihood-based comparison was performed among Poisson, classical Hawkes, and marked Hawkes models using Akaike Information Criterion (AIC) and Bayesian Information Criterion (BIC).

5.6.1. Statistical Goodness of Fit Assessment

To complement visual comparisons presented in preceding sections and provide a more rigorous assessment of model adequacy, likelihood-based benchmarking was performed using three arrival models: a memoryless Poisson process, a classical Hawkes process, and the proposed mark-dependent Hawkes framework. Model performance was evaluated using the log-likelihood, AIC, and BIC, which jointly assess model fit and complexity. The resulting statistics are summarized in Table 6.

The Poisson model produced the lowest log-likelihood and the highest AIC/BIC values, indicating poor agreement with the measured PLC impulsive noise. This observation is consistent with the KS goodness-of-fit results presented in Subsection 5.2, which rejected the exponential inter-arrival assumption associated with Poisson arrivals. In contrast, both Hawkes-based models achieved substantially improved likelihood scores, confirming the temporal dependence and self-excitation in the measured impulsive EMI process. This comparison demonstrates that self-exciting point process formulations provide a significantly more realistic representation of PLC impulsive noise than conventional memoryless models. The likelihood-based improvement obtained by Hawkes models supports the hypothesis that impulsive EMI arrivals occur in clusters rather than independently. Consequently, incorporating event interaction mechanisms is essential for accurately capturing the temporal structure of PLC noise. In this work, a Poisson process was selected as the baseline benchmark because it represents the classical memoryless arrival assumption, providing a reference against which the benefits of temporal clustering and self-excitation can be quantified.

5.7. Engineering Implications for PLC Systems

The statistical characteristics identified in this study have important implications for practical PLC system design. The rejection of the Poisson arrival assumption and the superior performance of Hawkes-based models indicate that impulsive EMI arrivals exhibit temporal clustering and short-term memory, implying that conventional memoryless noise models may underestimate burst-error occurrence in PLC links. Such behaviour is consistent with interference generated by switching power supplies, inverter-based systems, motor drives, and other nonlinear electrical loads commonly present in modern power networks. Furthermore, the EVT analysis confirms significant impulsive amplitude variations, highlighting the need for robust coding, adaptive modulation, and impulsive-noise mitigation techniques capable of handling extreme interference events. The proposed marked self-exciting framework therefore provides a physically meaningful basis for realistic EMI simulation and performance evaluation of next-generation PLC systems operating in increasingly complex electromagnetic environments.

From an engineering perspective, the proposed framework provides a practical tool for generating realistic synthetic impulsive noise sequences that preserve both temporal clustering and amplitude statistics observed in measured PLC environments. Such synthetic noise models can be used to evaluate receiver performance, bit-error-rate (BER) behaviour, coding schemes, and modulation strategies under realistic EMI conditions. In addition, the explicit representation of temporal excitation enables the development of adaptive and predictive interference mitigation algorithms capable of anticipating bursty impulsive events and dynamically adjusting receiver parameters to improve communication reliability. The estimated conditional intensity may be used as a real-time indicator of impulsive-noise risk, enabling adaptive activation of blanking, filtering, or error-control mechanisms. In addition, the proposed framework can generate realistic synthetic PLC noise for receiver evaluation and BER performance testing.

6. CONCLUSIONS

This study presents a marked self-exciting point process framework for modeling bursty impulsive noise in PLC systems, integrating both temporal dynamics and amplitude characteristics within a unified statistical structure. The analysis of measured PLC data demonstrated that impulse arrivals exhibit short-term temporal dependence and clustering, as evidenced by skewed inter-arrival distributions, nonlinear CCDF behavior, and nonzero autocorrelation at small lags, deviating from the memoryless assumption of Poisson processes. The parameter estimation results showed stable baseline activity with moderate excitation effects and rapid decay, indicating that the noise process was primarily driven by persistent background interference with localized temporal interactions. Amplitude analysis revealed a skewed distribution with intermittent high-energy events, whereas EVT-based modeling indicated bounded tail behavior, suggesting that extreme impulses are present but not unbounded. Validation on unseen datasets confirmed the robustness and generalization capability of the proposed framework, with consistent temporal and amplitude characteristics observed without parameter re-estimation. A comparative analysis further showed that conventional Poisson models failed to capture observed dynamics, with a measurable CCDF deviation (error $= 0.15932$), highlighting the importance of incorporating temporal dependence in PLC noise modeling. Overall, the proposed model provides a realistic and physically interpretable representation of impulsive electromagnetic interference in transmission lines, offering a solid foundation for designing adaptive and resilient PLC communication systems. Future work will investigate online and adaptive parameter estimation techniques to enable real-time implementation of the proposed framework in dynamic PLC environments, nonstationary and regime-switching extensions of the proposed framework, alternative excitation kernels for long-memory impulsive processes, and integration of the model into PLC system simulations for communication performance assessment and adaptive interference mitigation.

ACKNOWLEDGEMENT

This work was supported by the Durban University of Technology under the Harnessing Talent (HANT) Postdoctoral Fellowship (PDF) Program. We also acknowledge Prof. Thomas Afullo from the University of KwaZulu-Natal for allowing the use of the measurement data in this research.

REFERENCES

[1] Zimmermann, M. and K. Dostert, "Analysis and modeling of impulsive noise in broad-band powerline communications," *IEEE Transactions on Electromagnetic Compatibility*, Vol. 44, No. 1, 249–258, Feb. 2002.

[2] Meng, H., Y. L. Guan, and S. Chen, "Modeling and analysis of noise effects on broadband power-line communications," *IEEE Transactions on Power Delivery*, Vol. 20, No. 2, 630–637, Apr. 2005.

[3] Middleton, D., "Statistical-physical models of electromagnetic interference," *IEEE Transactions on Electromagnetic Compatibility*, Vol. EMC-19, No. 3, 106–127, Aug. 1977.

[4] Katayama, M., T. Yamazato, and H. Okada, "A mathematical model of noise in narrowband power line communication systems," *IEEE Journal on Selected Areas in Communications*, Vol. 24, No. 7, 1267–1276, Jul. 2006.

[5] Chelangat, F. and T. Afullo, "Time series modelling of powerline communication impulsive noise: Queuing theory approach," *Progress In Electromagnetics Research C*, Vol. 150, 157–168, 2024.

[6] Corripio, F. J. C., J. A. C. Arrabal, L. D. del Rio, and J. T. E. Munoz, "Analysis of the cyclic short-term variation of indoor power line channels," *IEEE Journal on Selected Areas in Communications*, Vol. 24, No. 7, 1327–1338, Jul. 2006.

[7] Galli, S. and T. Banwell, "A novel approach to the modeling of the indoor power line channel-Part II: Transfer function and its properties," *IEEE Transactions on Power Delivery*, Vol. 20, No. 3, 1869–1878, 2005.

[8] Awino, S. O. and B. Nleya, "Power line communication: Extreme noise events modelling and characterization over low-voltage networks," *Progress In Electromagnetics Research C*, Vol. 162, 242–251, 2025.

[9] Ferreira, H. C., L. Lampe, J. Newbury, and T. G. Swart, *Power Line Communications: Theory and Applications for Narrowband and Broadband Communications over Power Lines*, John Wiley & Sons, 2011.

[10] Nassar, M., K. Gulati, Y. Mortazavi, and B. L. Evans, "Statistical modeling of asynchronous impulsive noise in powerline communication networks," in *2011 IEEE Global Telecommunications Conference — GLOBECOM 2011*, 1–6, Houston, TX, USA, 2011.

[11] Banelli, P., "Bayesian estimation of a Gaussian source in Middleton's class-A impulsive noise," *IEEE Signal Processing Letters*, Vol. 20, No. 10, 956–959, Oct. 2013.

[12] Lin, J., M. Nassar, and B. L. Evans, "Impulsive noise mitigation in powerline communications using sparse Bayesian learning," *IEEE Journal on Selected Areas in Communications*, Vol. 31, No. 7, 1172–1183, Jul. 2013.

[13] Awino, S. O. and B. Nleya, "Ensemble-based short-window nonlinear dynamical characterization of PLC impulsive noise," *Applied Sciences*, Vol. 16, No. 7, 3573, 2026.

[14] Nikias, C. L. and J. M. Mendel, "Signal processing with higher-order spectra," *IEEE Signal Processing Magazine*, Vol. 10, No. 3, 10–37, Jul. 1993.

[15] Awino, S. O. and B. Nleya, "Multifractal random walk model for bursty impulsive PLC noise," *Applied Sciences*, Vol. 16, No. 1, 49, 2026.

[16] Asiyo, M. O. and T. J. O. Afullo, "Analysis of bursty impulsive noise in low-voltage indoor power line communication channels: Local scaling behaviour," *SAIEE Africa Research Journal*, Vol. 108, No. 3, 98–107, Sep. 2017.

[17] Gianaroli, F., F. Pancaldi, E. Sironi, M. Vigilante, G. M. Vitetta, and A. Barbieri, "Statistical modeling of periodic impulsive noise in indoor power-line channels," *IEEE Transactions on Power Delivery*, Vol. 27, No. 3, 1276–1283, Jul. 2012.

[18] Nassar, M., J. Lin, Y. Mortazavi, A. Dabak, I. H. Kim, and B. L. Evans, "Local utility power line communications in the 3–500 kHz band: Channel impairments, noise, and standards," *IEEE Signal Processing Magazine*, Vol. 29, No. 5, 116–127, 2012.

[19] Deng, H., L. Liu, J. Xu, and T. Liu, "Deep learning-based impulsive noise detection and impulsive-noise-aware receiver for dft-s-ofdm systems," *IEEE Transactions on Cognitive Communications and Networking*, Vol. 12, 2455–2470, 2025.

[20] Jeong, J. J. and S. Kim, "Robust adaptive filter algorithms against impulsive noise," *Circuits, Systems, and Signal Processing*, Vol. 38, No. 12, 5651–5664, 2019.

[21] Daley, D. J. and D. Vere-Jones, *An Introduction to the Theory of Point Processes: Volume I: Elementary Theory and Methods*, Springer, 2003.

[22] Daley, D. J. and D.Vere-Jones, *An Introduction to the Theory of Point Processes: Volume II: General Theory and Structure*, Springer, 2008.

[23] Rasmussen, J. G., "Bayesian inference for Hawkes processes," *Methodology and Computing in Applied Probability*, Vol. 15, No. 3, 623–642, 2013.

[24] Hawkes, A. G., "Spectra of some self-exciting and mutually exciting point processes," *Biometrika*, Vol. 58, No. 1, 83–90, 1971.

[25] Coles, S., J. Bawa, L. Trenner, and P. Dorazio, *An Introduction to Statistical Modeling of Extreme Values*, Springer, 2001.

[26] Pickands III, J., "Statistical inference using extreme order statistics," *The Annals of Statistics*, Vol. 3, No. 1, 119–131, 1975.

[27] Ogata, Y., "Statistical models for earthquake occurrences and residual analysis for point processes," *Journal of the American Statistical Association*, Vol. 83, No. 401, 9–27, 1988.

[28] ETSI, "Powerline telecommunications (PLT); Coexistence between PLT modems and short wave radio broadcasting services," [Online]. Available: https://www.etsi.org/deliver/etsi_ ts /102500_102599/102578/01.02.01_60/ts_102578v010201p.pdf, 2008.

[29] Antoniali, M., F. Versolatto, and A. M. Tonello, "An experimental characterization of the PLC noise at the source," *IEEE Transactions on Power Delivery*, Vol. 31, No. 3, 1068–1075, Jun. 2016.

[30] Tlich, M., A. Zeddam, F. Moulin, and F. Gauthier, "Indoor power-line communications channel characterization up to 100 MHz — Part II: Time-frequency analysis," *IEEE Transactions on Power Delivery*, Vol. 23, No. 3, 1402–1409, Jul. 2008.

[31] Emleh, A., A. S. D. Beer, H. C. Ferreira, and A. J. H. Vinck, "The influence of fluorescent lamps with electronic ballast on the low voltage PLC network," in *2014 IEEE 8th International Power Engineering and Optimization Conference (PEOCO2014)*, 276–280, Langkawi, Malaysia, Mar. 2014.